Paper 2

Sensitivity of ground motion simulations to earthquake source parameters: a case study for Istanbul, Turkey

Sørensen, M.B., Atakan, K. and Pulido, N.

Sensitivity of ground motion simulations to earthquake source parameters: a case study for Istanbul, Turkey

Mathilde B. Sørensen[1], Nelson Pulido[2], Kuvvet Atakan[1]

[1]Department of Earth Science, University of Bergen, Norway

[2]National Research Institute for Earth Science and Disaster Prevention, Earthquake Disaster Mitigation Research Center (NIED - EDM), Kobe, Japan

Corresponding author:

Mathilde B. Sørensen, Department of Earth Science, University of Bergen, Allegt. 41, N-5007 Bergen, Norway, phone: +47-55588755, e-mail: mathilde.sorensen@geo.uib.no, fax: +47-55583660

Abstract

Following the disastrous earthquakes in Izmit and Düzce along the North Anatolian Fault in 1999, the earthquake hazard in the Istanbul area became a great concern. In this study we simulate strong-ground motions caused by a scenario earthquake (M=7.5) in the Marmara Sea, and investigate the effect of varying the input parameters on the broadband frequency ground motion. Simulations are based on a multiasperity source model that involves the combined rupture of the North Anatolian fault segments beneath the Marmara Sea. We use a hybrid model combining a deterministic simulation of the low frequencies (0.1-1.0 Hz) with a semi-stochastic simulation of the high frequencies (1.0-10.0 Hz). Computation at each frequency range is performed separately and the total ground motion is combined in the time domain. We calculate a total of 16 earthquake scenarios corresponding to different source and attenuation parameters to study their effect on the ground motion. The most significant parameters in terms of ground shaking level are the rise time, rupture velocity, rupture initiation point and stress drop. The largest variability of strong ground motions is observed in adjacent regions to asperities and are associated with frequencies above 5Hz. For lower frequencies our simulated velocity spectra within the Istanbul area are fairly stable among scenarios.

Introduction

The city of Istanbul is under a significant seismic hazard due to its close proximity to the Marmara Sea segment of the North Anatolian Fault (NAF) (Figure 1). During the last century there has been a westward migration of large, destructive earthquakes along the NAF with the latest events occurring in Izmit and Ducze in 1999 (e.g. Barka et al., 1999). Following these large earthquakes, there has been an increase in the coulomb stress along the Marmara Sea segment (Hubert-Ferrari et al., 2000) which, together with the fact that no large earthquakes have occurred at least since 1766 (Barka et al., 2002), indicates that a large earthquake is likely to break this part of the NAF within the life time of the present city environment (Parsons et al., 2000; Parsons, 2004).

Seismic hazard in Istanbul has previously been estimated using probabilistic methods (Atakan et al., 2002; Erdik et al., 2004). For future risk mitigation and city planning, a reliable estimate of the seismic hazard in Istanbul is needed. Recently, increased knowledge on the NAF within the Marmara Sea allowed other methods to be applied. Pulido et al. (2004) modeled the bedrock ground motions due to a finite extent scenario earthquake source (M=7.5) in the Marmara Sea using a hybrid broadband simulation technique, and hereby gave a first insight to the complexity of ground shaking to be expected in a future earthquake. Such results are important because of their direct engineering implications. However, the uncertainties related to defining the source parameters of a scenario earthquake influence the results in a way which is until now not well resolved. Our main objective is therefore to study and quantify the effect of these uncertainties.

In the present study we simulate ground motions due to a number of earthquake scenarios in the Marmara Sea and compare to a reference scenario. The tested scenarios (15 in total) are defined by changing the critical source parameters one at a time to see their influence on the simulated ground motions. This provides important information about the sensitivity of the ground motions to the different source parameters and reveals the most critical ones.

Tectonic setting

The NAF is a ca 1200 km long fault structure extending through the northern part of Turkey from Erzincan in the East to the Aegean Sea in the West. The structure forms the boundary between the westward moving Anatolian Block with respect to the Eurasian plate, accommodating the relative motion through right-lateral strike-slip motion. In the westernmost part, around the Marmara Sea, the NAF splits into two main branches (Figure 1). Studying GPS displacement vectors, Okay et al. (2000) showed that the main strain accumulation takes place along the northernmost fault branch, which is therefore the target of our ground motion modeling. This northernmost fault branch consists of two main segments, namely the Central Marmara Fault (CMF) and the North Boundary Fault (NBF). The CMF has a strike almost parallel to the general stress orientation in the region and is therefore expected to break in a pure strike-slip earthquake. The NBF, on the other hand, is oblique to the stress orientation and constitutes a releasing bend on the NAF. We therefore expect an oblique normal mechanism along this segment. The velocity of the regional plate motion is approximately 2 cm/yr (Straub et al., 1997). Major historic earthquakes along these segments of the NAF include the 1509 earthquake (M=7.2) and the 1766 earthquake sequence (M=7.1 and M=7.4). In addition, a M=6.4 earthquake has ruptured along the NBF in 1963 (Ambraseys and Jackson, 2000).

Ground motion simulation methodology

We follow the approach of Pulido and Kubo (2004) and Pulido et al. (2004), using a hybrid method for modeling the ground motion. This procedure combines a deterministic simulation at low frequencies (0.1-1 Hz) with a semi-stochastic simulation at high frequencies (1-10 Hz). A finite-extent scenario earthquake source embedded in a flat-layered 1D velocity structure is assumed. The source consists of a number of asperities, which are divided into subfaults assumed to be point sources. The total ground motion at a given site is obtained by summing the contributions from the different subfaults. For the low frequencies, subfault contributions are calculated using discrete wave number theory (Bouchon, 1981) and summed assuming a given rupture velocity. At high frequencies, the subfault contributions are calculated using a stochastic method that incorporates a frequency-dependent radiation pattern by applying a smooth transition from a theoretical double-couple at low frequencies to a uniform radiation pattern at high frequencies following Pulido and Kubo (2004). Point sources are summed using the empirical Greens function method of Irikura (1986).

The ground motion simulations are performed at bedrock level and therefore do not take local site effects into account. This is important to keep in mind when interpreting the simulation results since local site effects are indeed present and important, especially in the southwestern part of the city (e.g. Birgören et al., 2004; Sørensen et al., in review). This issue is being addressed by Sørensen et al. (in review), aiming to combine ground motion simulation results with information about local site effects.

As input for the modeling, the source needs to be defined in terms of the location of the rupturing fault and its asperities together with asperity parameters such as rise time, rupture velocity, stress drop and seismic moment. Also the properties of the surrounding crust need to be defined giving velocity structure and attenuation characteristics.

Input scenarios

In order to provide a comparison between the different scenario results we have defined a reference scenario. The details of this scenario are explained below. The location and dimensions of the rupturing fault are defined by considering the local tectonics and seismicity. We assume a combined rupture of the CMF and NBF segments of the NAF. A total fault length of 130 km is used, which is confined to the area between the 1999 Izmit rupture to the east and the 1912 Ganos rupture to the west (Figure 1). We assume a fault width of 20 km in agreement with the depth of the seismogenic zone as indicated by the depth distribution of seismicity (Gurbuz et al., 2000). The fault plane solution used is the one of Pulido et al. (2004) with pure right-lateral strike-slip faulting along the CMF and an oblique-normal mechanism along the NBF. Two asperities are defined covering 22% of the fault plane following the empirical results of Somerville et al. (1999). These are located near the intersection of the CMF and NBF segments (Figure 1). This area has previously been suggested to be a seismic gap (Gurbuz et al., 2000), characterized by its low seismicity. The seismic moment released by the scenario earthquake is 2.0×10^{20} Nm, which is an average value of the seismic moments estimated by different authors for the 1999 Izmit earthquake (Pulido et al., 2004). The velocity model used in the modelling is the one used for routine location of earthquakes in the region (Figure 2). For the cut-off frequency f_{max} we use a value

of 10 Hz, which is also the upper frequency limit of the calculations. In practice this implies that the high-frequency decay of the ground motion is mainly controlled by attenuation.

For the reference scenario, the rupture initiation point is located in the westernmost edge of asperity 1 (Figure 1). This is believed to be a likely location since the boarder regions of asperities represent significant changes in physical properties of the fault and thereby zones of weakness. Based on seismic moment, fault area and asperity area, the stress drop is calculated following Pulido et al. (2004). Rupture velocity and rise time are taken from Pulido et al. (2004) for the reference scenario. The regional attenuation is defined in terms of Q. For the reference scenario we have used the "Low Attenuation Model" of Pulido et al. (2004). The source parameters of the reference scenario are summarized in Table 1. It should be noted that the reference scenario is considered as a conservative approximation.

Based on the reference scenario, we have changed source and attenuation parameters one by one in order to test their effect on the ground motions. For this purpose we simulate ground motions in the study area for each scenario and calculate their difference to PGA and PGV of the reference scenario. The parameters to be tested are attenuation (Q), rise time, rupture velocity, rupture initiation point and stress drop. In total, 15 "test scenarios" have been investigated, which are listed in Table 2.

Simulation results

The simulated PGA and PGV values for the reference scenario are shown in Figure 3. The largest accelerations are predicted in the southernmost part of the city, which is also located closest to the rupturing fault. Here we can expect bedrock accelerations of 0.5g or more in

some places. There is a very strong forward directivity effect on the ground motions, which is especially evident in the PGV distribution. Largest velocities are expected in the southeastern part of the city, where we predict velocities up to 125 cm/s. Due to the forward directivity, the shaking is extended far towards East from the rupturing fault which may have important implications along the populated areas around the Izmit gulf.

Variability in Q

In scenarios 1a, 1b and 1c we have tested the effect of attenuation by varying Q (Figure 4). In the ground motion simulations we use a frequency dependent Q defined by a relationship of the form $Q=Q_0 \cdot f^a$. In scenario 1a, we change the frequency dependency of the attenuation, coefficient a, using a=0.5 (a=1.5 for reference scenario). This implies lower values of Q for the higher frequencies, which implies higher attenuation of the seismic waves. For scenario 1a we see a reduction of PGA over a large area with a magnitude of up to 0.35g in comparison to the reference scenario. For the PGVs, the effect is smaller (maximum difference of 35 cm/s compared to reference scenario), but there is a tendency of increased PGVs in the forward directivity direction and decreased PGVs in the backward directivity direction. In scenario 1b we increase Q_0 to a value of 250 (Q_0=100 for reference scenario). This causes a general increase of Q, which implies reduced attenuation. The simulation results are in agreement with these considerations. For scenario 1b there is a general slight increase in PGA over the study area with a magnitude of up to 0.07g. The effect on PGV is mainly in the distribution of the ground motions. At asperity 1 there is a strong increase in PGV whereas the PGV decreases further eastwards at asperity 2, maximum change is at the order of 100 cm/s. Little effect is seen away from the fault. For the sake of comparison we have defined a scenario (scenario 1c) by combining scenarios 1a and 1b ($Q=250 \cdot f^{0.5}$). The effect of using this

attenuation relation is a reduction in PGA (up to 0.15g) distributed over a large area around the ruptured fault. The effect on the PGVs is decreased velocities in the forward directivity direction. This indicates that the frequency dependency (coefficient a) has the largest effect on the high-frequency ground motion by controlling peak accelerations whereas Q_0 has the main effect on the low-frequency ground motion by controlling peak velocities.

Variability in rise time

In scenarios 2a-c (Figure 5), the influence of the rise time on the ground motion was tested by simulating ground motions with constant rise times of 2 s (scenario 2a) and 4 s (scenario 2b) and with randomly varying values between 2 and 4 s (scenario 2c) and comparing to the reference scenario with a rise time of 3s. The effect of the rise time on the PGVs is clear. Increasing the rise time decreases the PGV and vice versa. The effect is most dominating in regions adjacent to the asperities where we see a change of up to ±170 cm/s relative to the reference scenario. The effect of using a randomly varying rise time is significantly smaller (change up to 10 cm/s) and more complex. The general trend is a reduction of PGV in the near field and an increase in the far field. The effect on the PGAs is more scattered and diffuse. The general trend is a scattered reduction in PGA for both reduced and increased rise time with the largest impact in regions adjacent to the asperities. Letting the rise time vary randomly also causes a reduction in PGA. In all cases, the maximum level of change is 0.5-0.6g.

Variability in rupture velocity

In scenarios 3a-c, the effect of the rupture velocity has been tested (Figure 6). In scenario 3a, the rupture velocity was reduced to 2.5 km/s (3.0 km/s for reference scenario), in scenario 3b

it was increased to 3.5 km/s and in scenario 3c we let the rupture velocity vary randomly between 2.5-3.5 km/s. The simulation results show that the rupture velocity has a strong effect on the PGVs, especially in the forward directivity direction. Increasing the rupture velocity also increases the PGV, whereas a reduction in rupture velocity causes reduced PGVs. Using the randomly varying rupture velocity causes a change in the PGV distribution with areas with decreased PGV being the dominating feature. The level of change for the PGV is up to 150 cm/s. For the PGAs a similar, but more scattered effect is seen. Reduction of rupture velocity reduces the PGAs whereas increased rupture velocity causes increased PGA. Using a random rupture velocity causes a slight redistribution of the ground motions near the fault. The level of maximum change for the PGAs is 0.6-0.7g or even higher in the region close to asperity 1 for scenario 3a.

Variability in rupture initiation point

The effect of changing the location of rupture initiation has been tested in scenarios 4a-d (Figure 7). In scenario 4a, the rupture initiation point (RIP) was moved to the intersection of the CMF and NBF segments of the rupturing fault. In scenario 4b, the RIP was located at the easternmost point of asperity 2 and for scenario 4c the RIP was located at the easternmost point of the NBF segment. In scenario 4d, the RIP was moved westwards to the westernmost point of the CMF. For all these scenarios, the hypocentral depth was held constant at 15 km for easy comparison. The simulation results show a clear effect of the location of the RIP on the distribution of the ground motion. For the PGVs, the effect of directivity is very clear and significant. For scenario 4a we see a reduction of PGV in the forward directivity direction of the reference scenario due to the changed direction of rupture along asperity 1. This also causes an increase in PGV towards the west. The same trend is seen more clearly for scenarios

4b and 4c where the RIP is moved successively further eastward. This completely changes the directivity pattern causing reduced PGVs to the east and increased PGVs to the west. For scenario 4d, moving the RIP westwards has a small effect on the simulated ground velocities. The magnitude of the change is up to 300 cm/s in all cases except scenario 4d where PGV changes on the order of 100 cm/s. For the PGA distribution, the same trend is present, but with more scatter due to the more incoherent nature of accelerations. The largest increases are observed close to the RIP of the reference scenario. For scenario 4d we observe a slight decrease in PGA close to the epicenter due to the directivity towards this region in the bilateral rupture of the reference scenario. The maximum magnitude of the variation varies between 0.4-0.7g for the four scenarios.

Variability in stress drop

The final test of this study was for the influence of stress drop on the ground motion distributions in scenarios 5a-b (Figure 8). In scenario 5a, the stress drop was reduced by 50% to 2.5 MPa for the background slip and 5 MPa for the asperities. In scenario 5b, the stress drop was increased by 50% to 7.5 MPa for the background slip and 15 MPa for the asperities. The effect is most significant on the PGA levels. Both PGV and PGA decrease when decreasing the stress drop and increase for an increased stress drop, affecting a larger area around the rupturing fault for PGA. The magnitude of the change is 30-40 cm/s for PGV and up to 0.5g for PGA. This implies that stress drop mainly affects high frequency incoherent ground motions.

Comparison of parameters

As shown above, several of the input parameters used in the ground motion simulations have a significant effect on the resulting ground motions, both in terms of distribution and absolute level of the ground motions. The location of the rupture initiation is critical due to the effects of directivity and, for the case of Istanbul, controls the distribution of very strong shaking in the densely populated areas of the city centre vs. offshore in the Marmara Sea.

The magnitudes of changes caused by varying the rise time and rupture velocity are on the same level. However, the natures of the changes are different in terms of the affected regions. The effect of rise time is mainly observed in adjacent regions to the asperities where most of the slip occurs, but also tends to distribute in the direction of rupture propagation. The rupture velocity, on the other hand, has an important effect along the whole rupture and the largest variations are seen along the forward directivity direction. In both cases the effect on PGA is scattered and in general distributed over larger regions than the PGVs.

Figure 9 shows the distribution of standard deviations in PGA and PGV based on all 16 scenarios. In general these two maps indicate that the largest variation in the standard deviation occurs close to the asperities. This is as expected since much of the variation in the ground motion is associated to the location of asperities and their input parameters. Their variation naturally affects the surrounding regions. The level of standard deviation of both PGA and PGV decreases gradually by increasing distance from the fault asperities. However, PGA variability is spread over a wider area compared to PGV variability.

Frequency distribution of ground motion and implications for engineering

When applying seismic hazard results to engineering problems, the frequency distribution of the ground motions becomes an important factor in addition to the peak ground motions. Therefore we have studied the frequency distribution of the ground motion simulation results at six sites in terms of maximum spectral velocity (SV) and response spectra. The locations of the sites (Figure 10) have been chosen to represent different parts of the city both in terms of land use, local geology and directivity of the simulated ground motions. Site PEN (Pendik) is located on the Asian side of the city in the forward directivity direction for the reference scenario. Site KUM (Kumköy) is north of the city at the Black Sea coast and is included for investigating the effect of distance on the spectra. Sites SIT (Avcilar) and ATA (Ataköy) are located in areas known to be affected by local site effects (Tezcan et al., 2002, Sørensen et al., in review). The remaining two sites, HIS and BUS, are located in the historical center (Sultanahmet) and the business center (Levent), respectively.

For each of the six sites, SV has been averaged in three frequency bands, namely f<1Hz, 1Hz<f<5Hz and f>5Hz. The limits of these frequency bands are chosen to coincide with the spectrum characteristic periods of the Turkish Design Code for various site classes (Aydinoglu, 1998). A large part of the building stock in Istanbul consists of 3-5 story buildings with resonance frequencies around 3-5 Hz. However, also a large number of medium-rise buildings susceptible to frequencies down to 1 Hz are present. Shaking at frequencies lower than 1 Hz affects mainly high-rise or long-span structures and therefore has less engineering implications in most parts of the city. Figures 11-13 show the comparisons of spectral values for each of the six sites. For each site, average SVs are computed for the reference scenario and each of the 15 test scenarios, and the absolute values are compared.

For the low frequencies (Figure 11), the most dominating parameters are rise time and rupture velocity (scenarios 2a-c and 3a-c). The influence of the rise time is significant at all the sites, whereas rupture velocity has little effect at the northernmost site (KUM), indicating that the effect of rupture velocity is only significant within a short distance to the fault. At higher frequencies, the variations in SV for these scenarios are negligible, indicating that even though these parameters cause large variations in the ground motion levels, their effect for engineering issues is limited in most parts of the town.

In the 1-5Hz frequency band (Figure 12) we see an effect of the rupture initiation point on the spectral values. This effect decreases for increased frequencies, indicating that the RIP mainly has an impact on the damage of large structures such as high-rise buildings. Another outstanding feature for this frequency band is the stress drop (scenarios 5a and 5b), which has a clear effect on the spectral values. From this we can conclude that the stress drop is an important parameter with large impact on the level of potentially damaging ground motion, which therefore should be given attention in future studies.

In Figures 11-13, the SV values are plotted for the EW and the NS components separately. For the high frequencies (f>5Hz), the amplitudes are almost identical for the two components, which is in agreement with the radiation pattern correction applied in the simulations (isotropic radiation pattern at high frequencies). However, at lower frequencies large differences are seen, especially in the forward directivity direction (PEN), which are probably a combined effect of the directivity and the double couple radiation of the low-frequency energy from the fault.

Response spectra in Istanbul

Figure 14 shows velocity response spectra for the 16 scenarios at the six sites of Figure 10. It is seen that both peak frequency and spectral level varies with azimuth and distance to the fault. The response spectra of the standard scenario are shown in the figure as black lines. At PEN (Figure 14a) we see a very strong peak at long periods (low frequencies) in the EW direction. This is expected to be due to the forward directivity of the ground motion. In general, at this site, we see maximum response spectra values at 0.2-0.3 Hz frequencies, which will have an effect on high-rise buildings in this area. Secondary peaks are seen around 2 Hz and 5 Hz, which will have a smaller absolute effect, but will affect lower rise buildings which are more common.

The response spectra for SIT and ATA (Figure 14b and 14c) are very similar, and differ significantly from the spectra at PEN. For these spectra we see a strong peak around 2 Hz which will be very critical for building damage in these densely populated areas largely occupied by ~5 story buildings, which have resonance frequencies around this value (Aydinogly, 1998). Since we expect significant site effects in this area with amplification also around this frequency (Sørensen et al., in review), the actual response can be even higher than predicted in this study. Again we also see peaks around 0.2 and 0.5 Hz which can affect high-rise buildings.

KUM (Figure 14d) is located far from the rupturing fault, which is also reflected in the response spectra having significantly lower values. The dominating peak is at low frequencies, 0.2-0.3 Hz, but also here amplitudes are low and little effect is predicted.

At HIS (Figure 14e), the Sultanahmet site, we also see a main peak at 0.2 Hz and a strong secondary peak at 2 Hz. This secondary peak will be critical for the building stock mainly consisting of old residential blocks of around 5 stories. The large number of historical monuments have much more complex response than simple quadratic modern residential buildings and may be vulnerable to a variety of frequency bands.

Finally, for the site BUS (Figure 14f) located in the business district of Istanbul, the strongest velocity response is seen at low frequencies (0.2-0.3 Hz) which is critical for the many high-rise buildings (40 stories and more) present in this area.

From an engineering perspective, an important result of the sensitivity analysis of this study is the effect of changing the scenario input parameters on the resulting response spectra. Despite the large variations between the various scenarios in terms of ground motion levels and distributions, the response spectra shown in Figure 14 are relatively similar for most scenarios. The general trend is that the variation increases for the low frequencies. For the peak frequencies we see a significant variation up to ±50 %, but this is only seen for a few scenarios. Generally, the variation between the response spectra is larger for sites close to the fault (SIT and ATA in Figures 14b and 14c), whereas much smaller variations are seen at larger distances (KUM and BUS in Figures 14d and 14f).

Figure 15 shows the distribution of standard deviation of the response spectra in three frequency bands based on the 16 scenarios. For the spectral accelerations (Figures 15 a-c) there is a strong frequency dependency of the standard deviations. At the low and intermediate frequencies (f<5Hz) standard deviation is small, whereas there is a remarkable variation between the scenarios for the high frequencies. For f>5Hz, standard deviations of up to 1g are

observed in the acceleration response spectra, and significant variation is distributed over a large area. For the velocity response spectra (Figure 15d-f), the standard deviation decreases rapidly with distance to the fault with a maximum spectral standard deviation of 10-15 cm/s in southern Istanbul. We see that the main variability in the standard deviation of velocity response spectra is associated with the low frequencies (f<1Hz). The similarity between the response spectra at low and intermediate frequencies implies that even if we are uncertain of the exact values of the input parameters for ground motion modeling, we still do a reasonably good job in predicting consistent response spectra up to frequencies around 5Hz. However, the large variation observed for frequencies above 5Hz, though less important in engineering applications, cannot be ignored.

Discussion

The results of this study reveal that even if we have reliable ground motion estimation methodologies we are still limited in the prediction of ground motions from future earthquakes by our limited knowledge of the source and attenuation parameters. This uncertainty is important and should always be kept in mind when interpreting ground motion simulation results. However, being aware of the uncertainties, ground motion simulations still provide a strong tool in determining seismic hazard levels in places with a high probability of exceedence.

When modeling ground motions from future earthquakes, one approach for dealing with the uncertainties is to define a number of scenarios with different values of the uncertain source parameters. For example, a "worst-case scenario" and a "best-case scenario" can be defined.

In this way, upper and lower limits of the expected ground motions can be defined and the user can choose the appropriate level of conservatism depending on the use of the results.

The most important parameters for the ground motion modeling, in terms of ground shaking levels, are the location of the rupture initiation, stress drop, rise time, rupture velocity and the anelastic attenuation for the studied region. However, the impact of these parameters in frequency bands of engineering interest varies. From an engineering perspective, the most important parameters are the stress drop and the location of rupture initiation. Also rupture velocity and rise time will play an important role due to their strong effect on PGV. Unfortunately, these parameters are difficult to predict for future earthquakes, but detailed studies should be made ahead of ground motion modeling, and in case of large uncertainties, extreme values should be considered in the input to the models to set bounds on the predicted ground motions.

The presented ground motions are all calculated at bedrock level and therefore do not take local site effects into account. When assessing the damage potential of a scenario earthquake at a given location, the local geology must be taken into consideration since the presence of e.g. soft sediments can both amplify the peak ground motions and shift the dominant frequencies of ground shaking. In this respect, the damage potential of the scenarios as discussed above, may be significantly modified by the inclusion of local site effects.

In the present study, we have used one of many methodologies for estimating ground motions due to a future large earthquake. We have tested the effect of changing the various input parameters but have not discussed the issue of variation among different ground motion

modeling methodologies. There are ongoing efforts in this end, and the discussion about these is out of the scope of this paper.

Conclusions

Based on our analysis of the effect of input parameters on ground motion simulation results we can draw the following conclusions:

- The expected effect of a M=7.5 earthquake in the Marmara Sea on the city of Istanbul will be significant with the largest ground motions occurring in the southern and southeastern parts of the city. Here, ground accelerations at the level of 0.5g and velocities above 50 cm/s can be expected at bedrock level.

- Rise time, rupture velocity, rupture initiation point and stress drop are the most significant parameters in terms of variations in ground shaking levels. However, these parameters have their effect in different frequency bands and their engineering significance therefore varies.

- High frequency ground motion is mainly controlled by the stress drop and Q. These parameters have a strong effect on PGA and PGA attenuation.

- Rupture velocity and rise time have a strong effect on the PGV values controlled by the coherent low frequency ground motion.

- For the selected sites in Istanbul, the response spectra consistently show peaks around 2Hz as well as at longer periods (4 sec). The combined effect of large PGA values at high frequencies and large PGV values at longer periods could have a strong effect on the damage potential of ground motion for a wide range of buildings in Istanbul.

- The largest variability of ground motion is observed in adjacent regions to asperities as well as in the direction of rupture propagation. For PGV values the variability rapidly

decreases with increasing distance to the fault. In the case of PGA values the variability is distributed over a much wider region.

- The variability of acceleration response spectra is strongly frequency dependent with a significant variation in the high-frequency part of the spectra. This reflects the dominance of high frequencies in ground motion accelerations.

- Even though the level, distribution and spectral values of the ground motions differ significantly, the velocity response spectra are consistent, revealing the strength of ground motion modeling in estimating a realistic hazard for Istanbul and hence in risk mitigation efforts despite the large uncertainties involved.

Our efforts in the future should focus on understanding the accuracy of the most critical parameters influencing the ground motion, namely the rise time, rupture velocity, rupture initiation point and the stress drop.

References

Ambraseys, N.N. and Jackson, J.A., 2000. Seismicity of the Sea of Marmara (Turkey) since 1500, *Geophys. J. Int.*, 141, F1-F6.

Atakan, K., Ojeda, A., Meghraoui, M., Barka, A.A., Erdik, M. and Bodare, A., 2002. Seismic Hazard in Istanbul following the 17 August 1999 Izmit and 12 November 1999 Düzce Earthquakes, Bulletin of the Seismological Society of America, 92, 466-482.

Aydinoglu, M.N., 1998. Specification for Structures to be Built in Disaster Areas, Part III – Earthquake Disaster Prevention, Ministry of Public Works and Settlement, Government of Republic of Turkey, Official Gazette, No. 23390.

Barka, A., Akyüz, H.S., Altunel, E., Sunal, G., Cakir, Z., Dikbas, A., Yerli, B., Armijo, R., Meyer, B., de Chabalier, J.B., Rockwell, T., Dolan, J.R., Hartleb, R. Dawson, T., Christofferson, S., Tucker, A., Fumal, T., Langridge, R., Stenner, H., Lettis, W., Bachhuber, J. and Page, W. (2002). The Surface Rupture and Slip Distribution of the 17 August 1999 Izmit Earthquake (M 7.4), North Anatolian Fault, Bulletin of the Seismological Society of America, 92, 1, 43-60.

Birgören, G., Özel, O., Fahjan, Y. and Erdik, M., 2004. Determionation of site effects in Istanbul area using a small earthquake record of the dense strong motion network, XXIX General Assembly of the European Seismological Commission, Potsdam, Germany, poster no. 249.

Bouchon, M. (1981): A simple method to calculate Green's functions for elastic layered media, Bull. Seism. Soc. Am., 71, 959-971.

Erdik, M., Demircioglu, M., Sesetyan, K., Durukal, E. And Siyahi, B., 2004. Earthquake hazard in Marmara Region, Turkey, Soil Dynamics and Earthquake Engineering, 24, 605-631.

Gurbuz, C., Aktar, M., Eyidogan, H., Cisternas, A., Haessler, H., Barka, A., Ergin, M., Turkelli, N., Polat, O., Ucer, S.B., Kuleli, S., Baris, S., Kaypak, B., Bekler, T., Zor, E., Bicmen, F., and Yoruk, A., 2000. The seismotectonics of the Marmara region (Turkey): results from a microseismic experiment. Tectonophysics, 316, 1-17.

Hubert-Ferrari, A., Barka, A., Jacques, E., Nalbant, S.S., Meyer, B., Armijo, R., Tapponnier, P. and King, G.C.P. (2000). Seismic hazard in the Marmara Sea region following the 17 August 1999 Izmit earthquake, Nature, 404, 269-273.

Irikura, K. (1986): Prediction of strong acceleration motion using empirical Green's function, Proceedings of the 7th Japan. Earthq. Eng. Symp., 151-156.

Okay, A.I., Kaslilar-Özcan, A., Imren, C., Boztepe-Güney, A., Demirbag, E. and Kuscu, I., 2000. Active faults and evolving strike-slip basins in the Marmara Sea, northwest Turkey: a multichannel seismic reflection study, *Tectonophysics*, 321, 189-218.

Parsons, T., Toda, S., Stein, R.S., Barka, A. and Dietrics, J.H., 2000. Heightened Odds of Large Earthquakes Near Istanbul: An interaction-Based Probability Calculation, Science, 288, 661-665.

Parsons, T., 2004. Recalculated probability of M ≥ 7 earthquakes beneath the Sea of Marmara, Turkey, Journal of Geophysical Research, 109, B05304, doi: 10.1029/2003JB002667.

Pulido, N. and Kubo, T. (2004): Near-fault strong motion complexity of the 2000 Tottori earthquake (Japan) from a broadband source asperity model , Tectonophysics, 390, 177-192.

Pulido, N., Ojeda, A., Atakan, K. and Kubo, T. (2004): Strong ground motion estimation in the Sea of Marmara region (Turkey) based on a scenario earthquake, Tectonophysics, 391, 357-374.

Somerville, P., Irikura, K., Graves, R., Sawada, S., Wald, D., Abrahamson, N., Iwasaki, Y., Kagawa, T., Smith, N., and Kowada, A., 1999. Characterizing crustal earthquake slip models for the prediction of strong ground motion. Seismol. Res. Lett., 70, 59-80.

Straub, C., Kahle, H.-G., Schindler, C., 1997. GPS and geologic estimates of the tectonic activity in the Marmara region, NW Anatolia. J. Geophys. Res. 102, 27 587–27 601.

Sørensen, M.B., Oprsal, I, Bonnefoy-Claudet, S., Atakan, K., Mai, P.M., Pulido. N. and Yalciner, C. (2005). Local site effects in Ataköy, Istanbul, Turkey, due to a future large earthquake in the Marmara Sea, submitted to Geophysical Journal International, June 2005.

Tezcan, S.S., Kaya, E., Bal, I.E. and Özdemir, Z., 2002. Seismic amplification at Avcilar, Istanbul, *Engineering Structures*, 24, 661-667.

Tables

Table 1: Source parameters for the reference scenario.

Hypocenter (Lat / Lon / Depth)	48.838°N / 28.519°E / 15 km
Seismic moment	$M_0 = 2.0 \cdot 10^{20}$ Nm
Strike / Dip / Slip CMF segment	81.5 / 90 / 180
Strike / Dip / Slip NBF segment	110 / 90 / -135
Average stress drop	5 MPa
Asperity stress drop	10 MPa
Rise time	3.0 s
Rupture velocity	3.0 km/s
f_{max}	10 Hz
Q	$100 \cdot f^{1.5}$

Table 2: Scenarios which have been tested in this study. Only the parameters differing from the reference scenario are listed.

Scenario 1a	$Q = 100 \cdot f^{0.5}$
Scenario 1b	$Q = 250 \cdot f^{1.5}$
Scenario 1c	$Q = 250 \cdot f^{0.5}$
Scenario 2a	Rise time 2.0 s
Scenario 2b	Rise time 4.0 s
Scenario 2c	Rise time random 3 ± 1 s
Scenario 3a	Rupture velocity 2.5 km/s
Scenario 3b	Rupture velocity 3.5 km/s
Scenario 3c	Rupture velocity random 3 ± 0.5 km/s
Scenario 4a	Rupture initiation at intersection of CMF and NBF
Scenario 4b	Rupture initiation at eastern edge of asperity 2
Scenario 4c	Rupture initiation at eastern edge of NBF
Scenario 4d	Rupture initiation at western edge of CMF
Scenario 5a	Stress drop asperity: 5 MPa, background: 2.5 MPa
Scenario 5b	Stress drop asperity: 15 MPa, background: 7.5 MPa

Figures

Figure 1: Map of active faulting in the Marmara Sea region (modified after Okay et al., 2000). The geometry of the reference scenario is given in the central Marmara Sea. The fault rupture is shown as a thick gray line, asperities are shown as darker gray line segments. The star shows the rupture initiation point.

Figure 2: Velocity model for the Marmara Sea region (Serif Baris, personal communication, 2003).

Figure 3: Simulation result for the reference scenario. a) PGA distribution, b) PGV distribution. Major faults are shown as grey lines and the rupture initiation point as a star.

Figure 4: Simulation results for scenarios 1a-c where the effect of attenuation is tested. The plots show the absolute difference in the ground motion values compared to the reference scenario. Major faults are shown as white lines and the rupture initiation point is shown as a star.

Figure 5: Simulation results for scenarios 2a-c where the effect of rise time is tested. The plots show the absolute difference in the ground motion values compared to the reference scenario. Major faults are shown as white lines and the rupture initiation point is shown as a star.

Figure 6: Simulation results for scenarios 3a-c where the effect of rupture velocity is tested. The plots show the absolute difference in the ground motion values compared to the reference

scenario. Major faults are shown as white lines and the rupture initiation point is shown as a star.

Figure 7: Simulation results for scenarios 4a-d where the effect of rupture initiation point is tested. The plots show the absolute difference in the ground motion values compared to the reference scenario. Major faults are shown as white lines and the rupture initiation point is shown as a star.

Figure 8: Simulation results for scenarios 5a-b where the effect of stress drop is tested. The plots show the absolute difference in the ground motion values compared to the reference scenario. Major faults are shown as white lines and the rupture initiation point is shown as a star.

Figure 9: Spatial distribution of standard deviation of a) PGA and b) PGV based on the 16 scenarios. Major faults are shown as grey lines and the rupture initiation point as a star.

Figure 10: Location of the six sites analyzed in terms of spectral velocity and spectral acceleration. The grey lines show the location of the major faults in the area and the star shows the rupture initiation point for the reference scenario.

Figure 11: Spectral velocity at the sites in Figure 20 in the frequency band f<1Hz. White bars represent the NS component of the ground motion and black bars represent the EW component.

Figure 12: Spectral velocity at the sites in Figure 20 in the frequency band 1Hz<f<5Hz. White bars represent the NS component of the ground motion and black bars represent the EW component.

Figure 13: Spectral velocity at the sites in Figure 20 in the frequency band f>5Hz. White bars represent the NS component of the ground motion and black bars represent the EW component.

Figure 14: Comparison of the velocity response spectra for all 16 scenarios. The reference scenario is shown as a thick black line. All three components are shown. x, y and z correspond to EW, NS and vertical, respectively. The various test scenarios are not differentiated in the plot since the aim is to show the variation and the upper and lower bounds of the spectra. a) PEN, b) SIT, c) ATA, d) KUM, e) HIS, f) BUS.

Figure 15: Distribution of standard deviation of response spectra for acceleration (a-c) and velocities (d-f). At each simulation point, the average value of the two horizontal components is used. The average response spectral values are shown in three frequency bands: a,d) f<1Hz, b,e) 1<f<5Hz and c,f) f>5Hz.
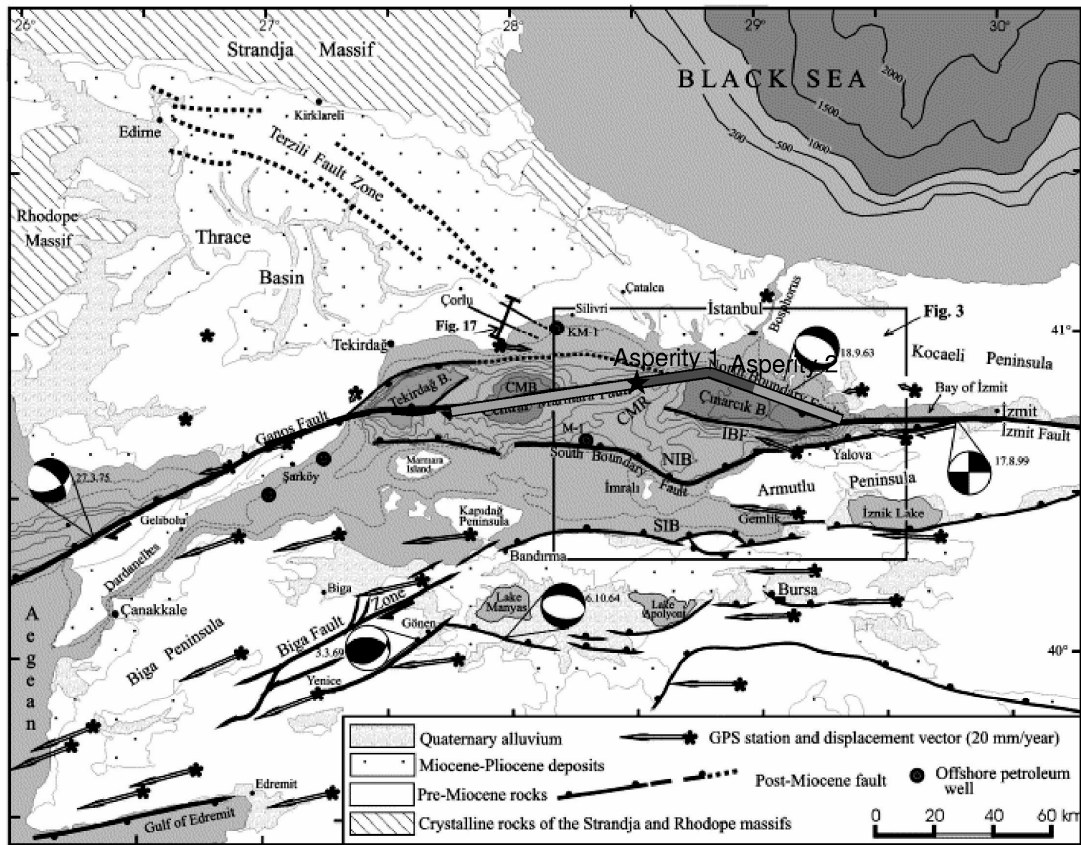
Figure 1.
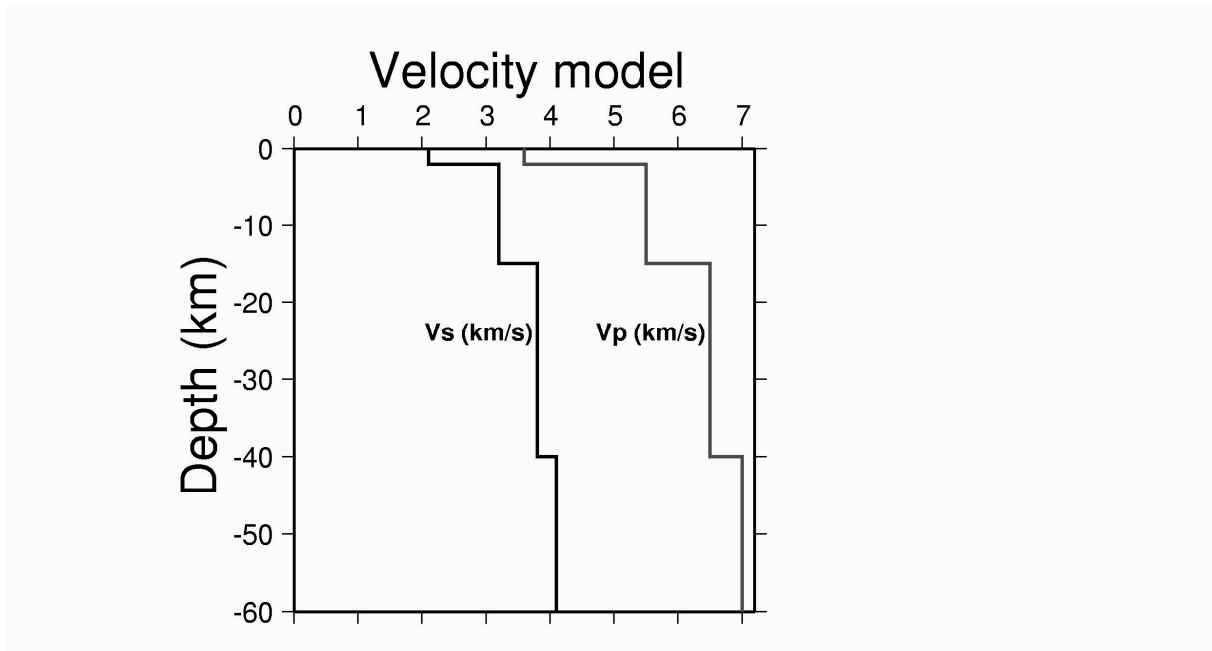
Figure 2.
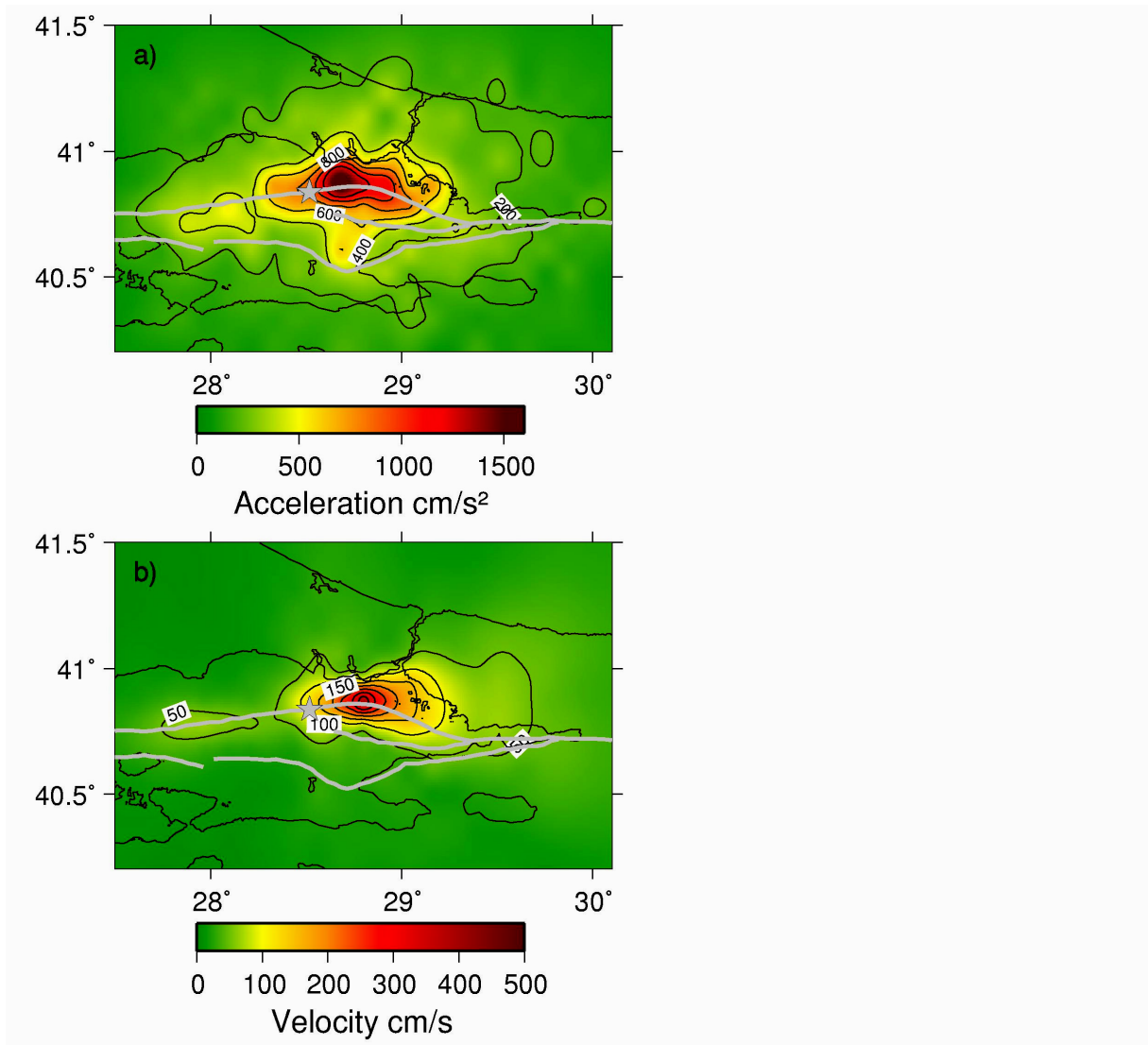
Figure 3.
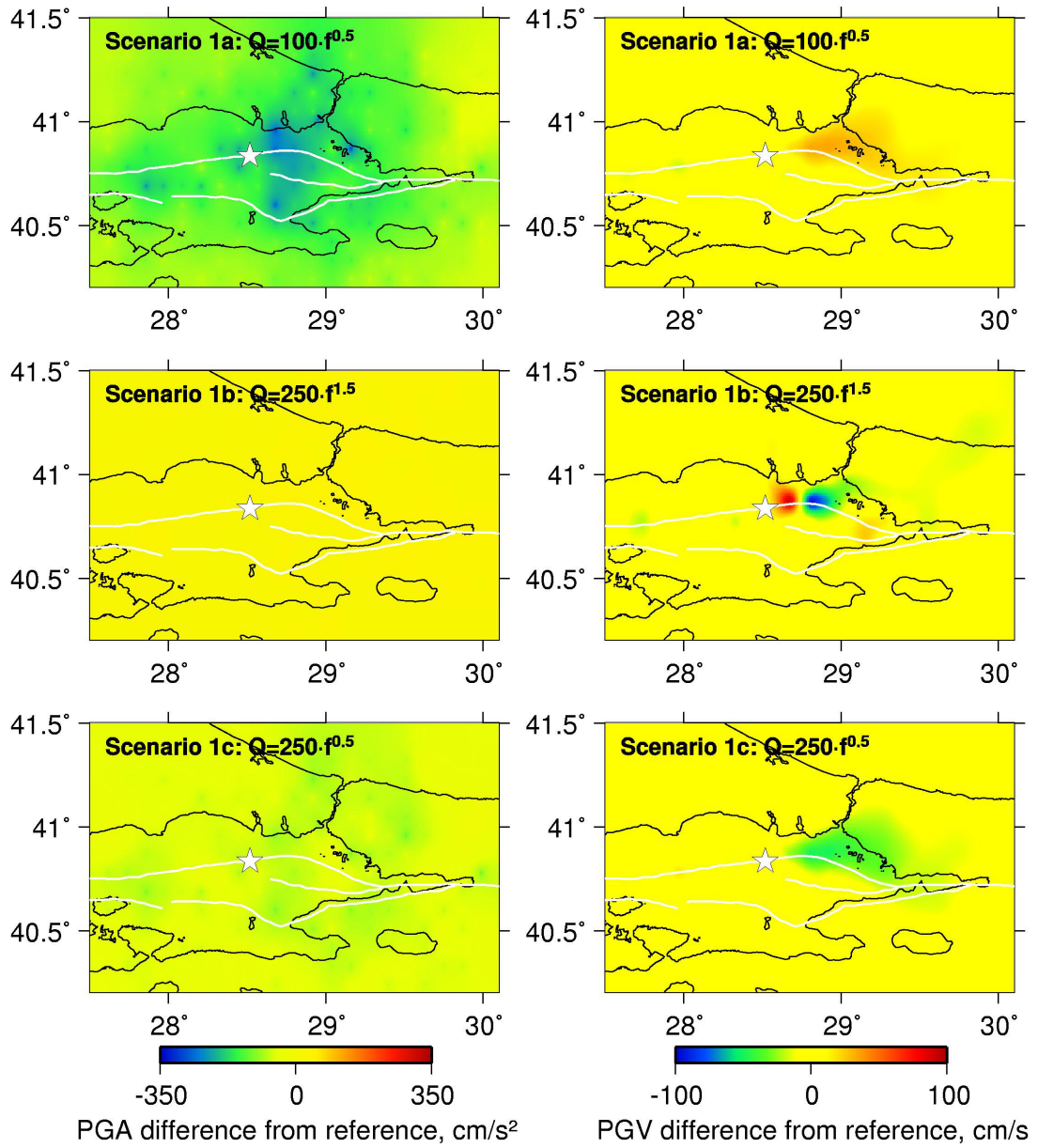
Figure 4.
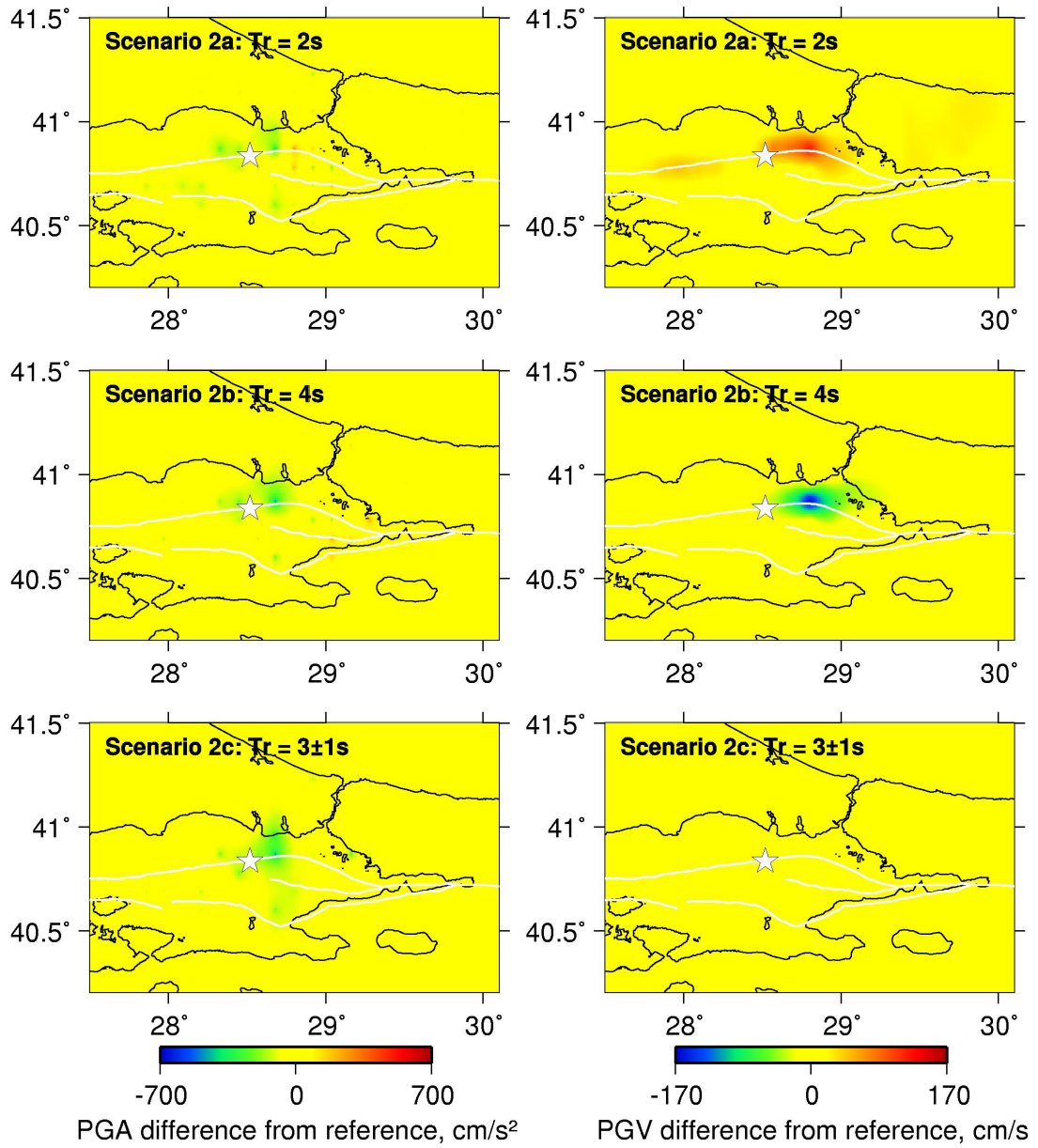
Figure 5.
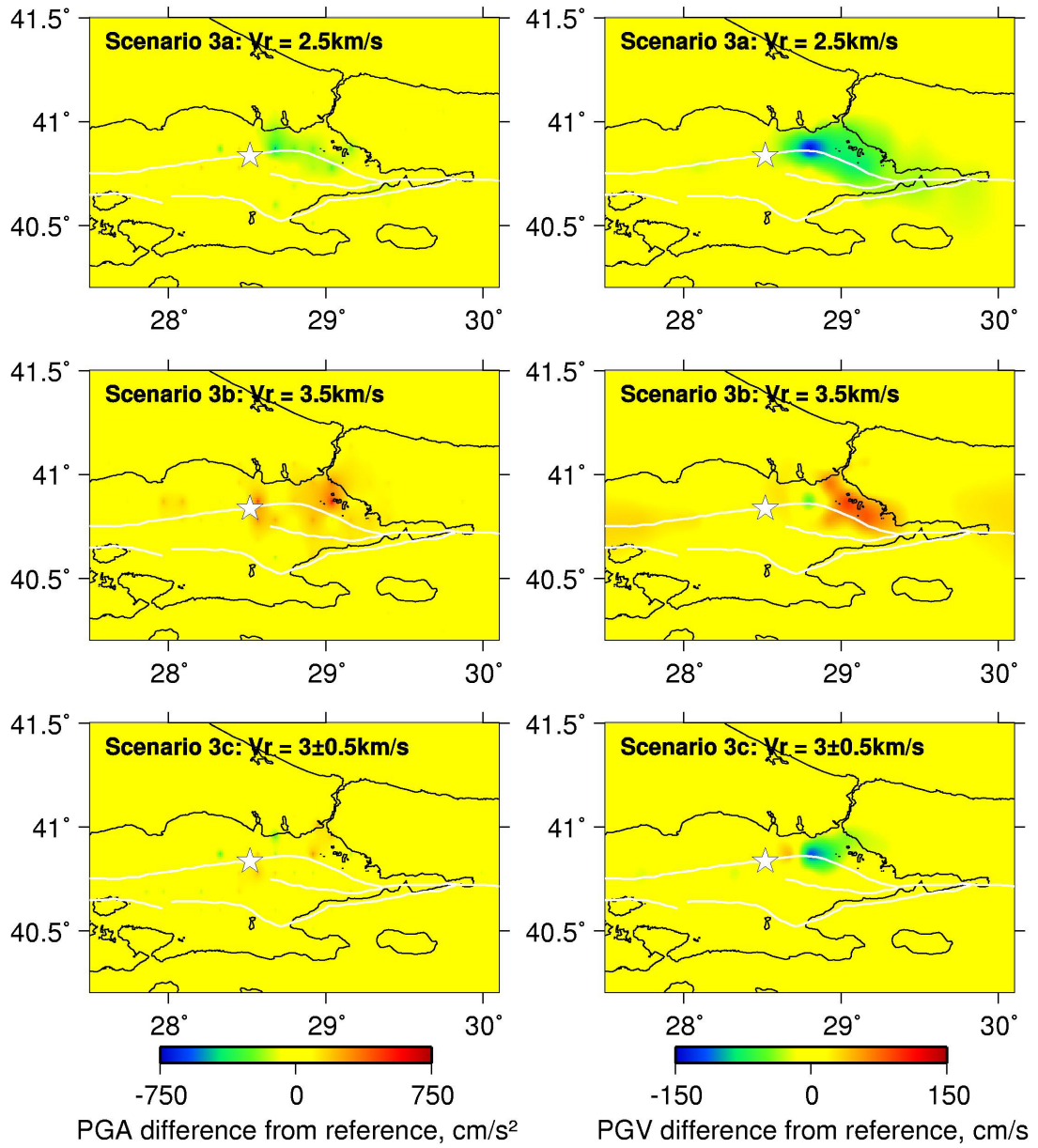
Figure 6.
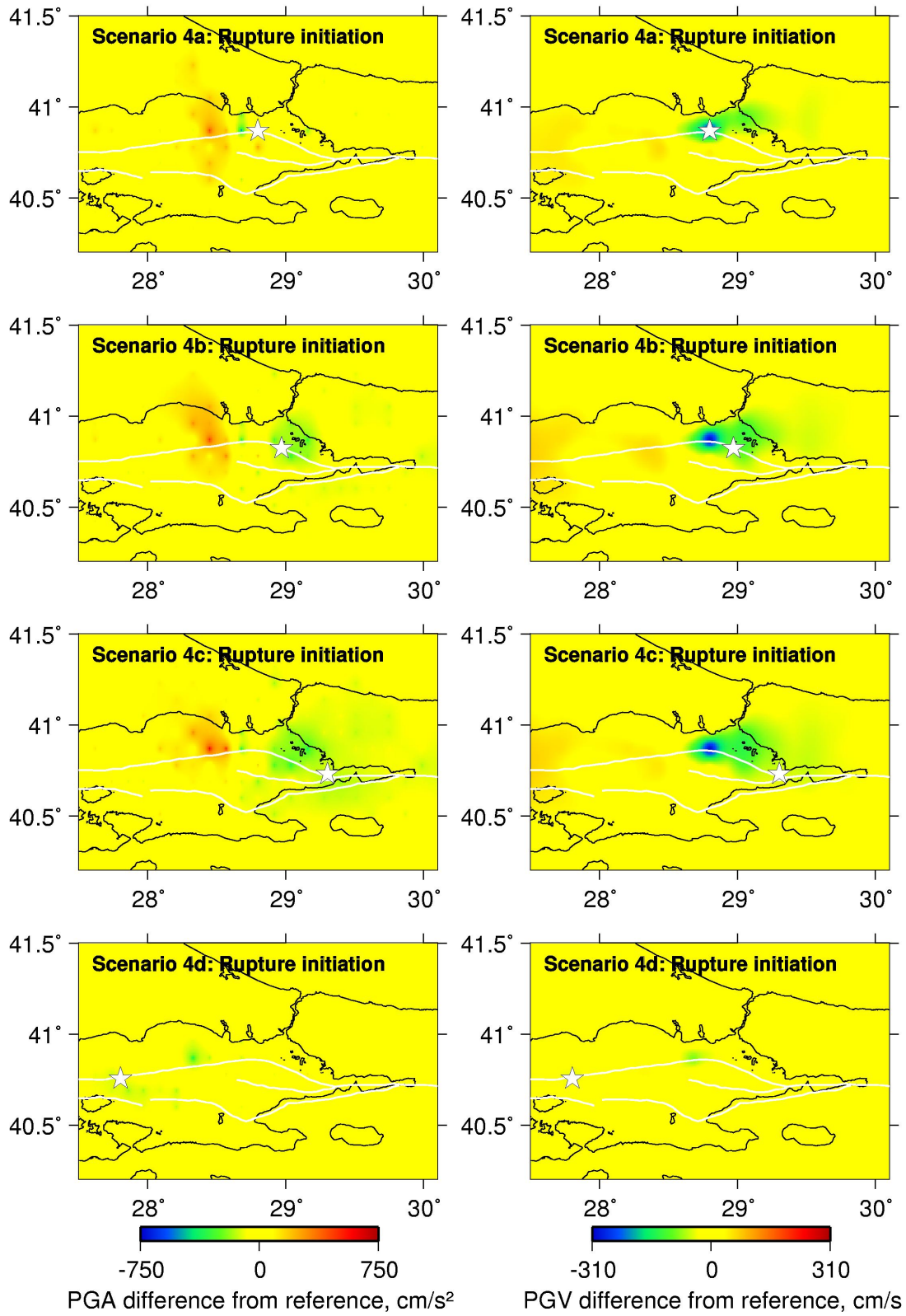
Figure 7.
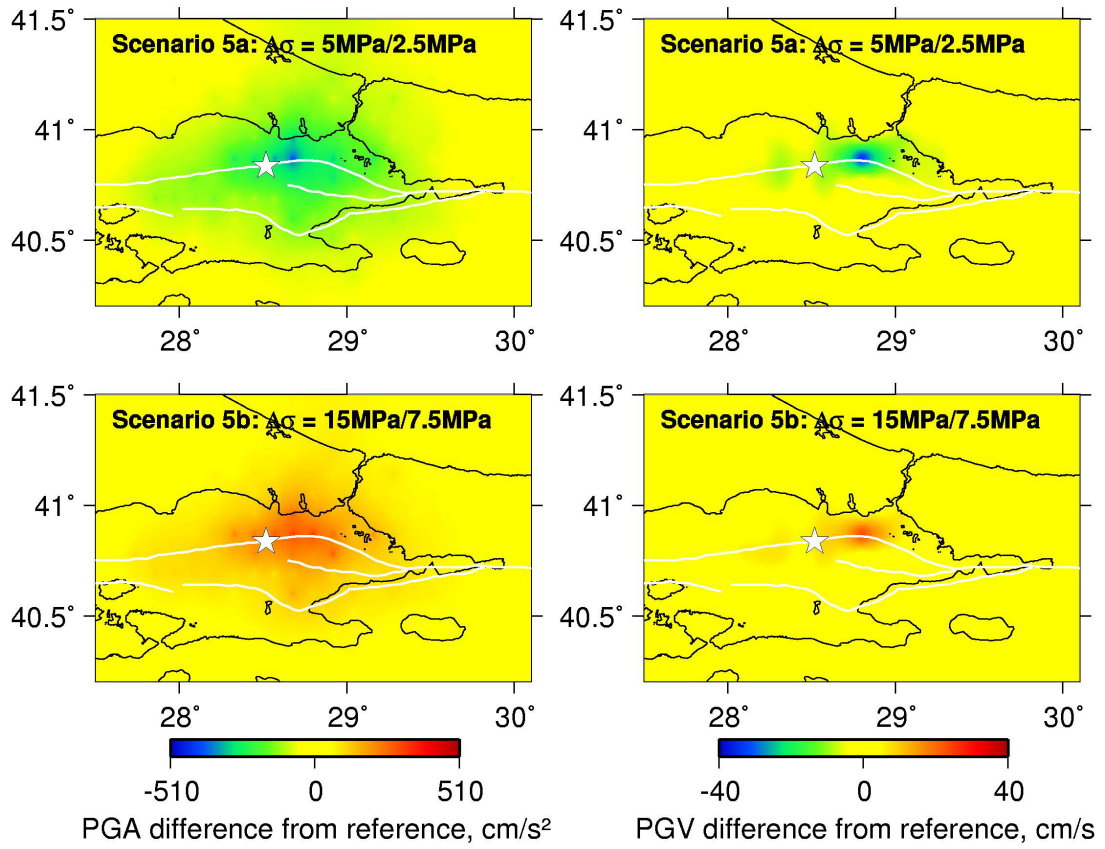
Figure 8.
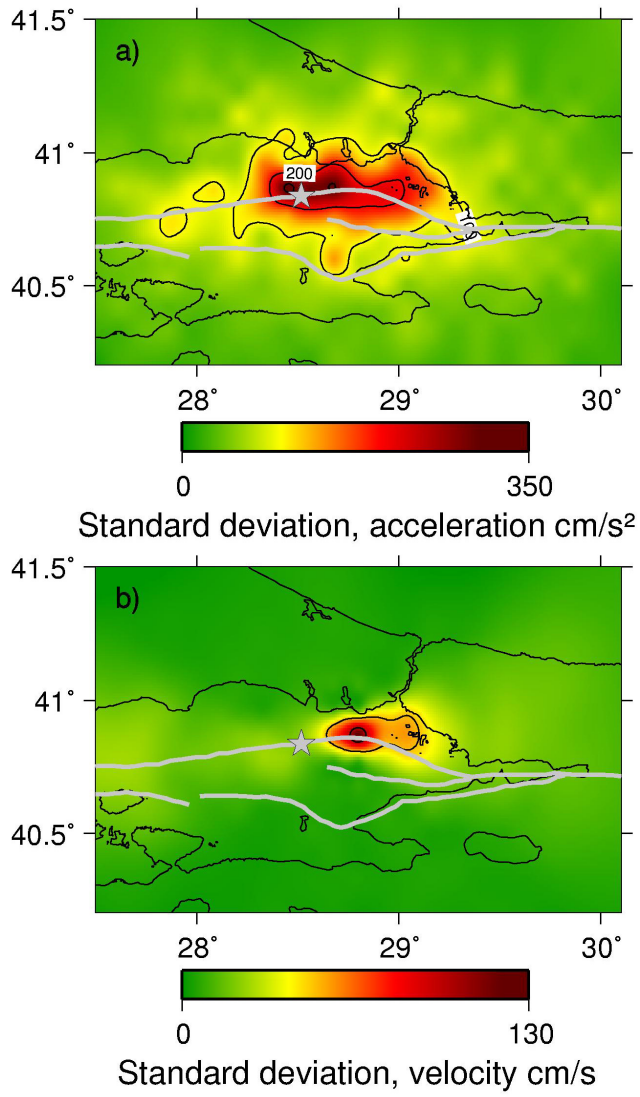
Figure 9.
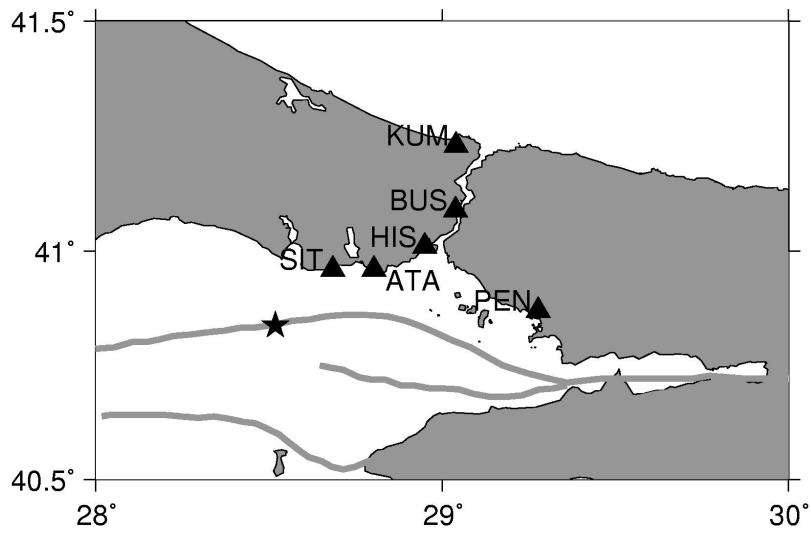
Figure 10.
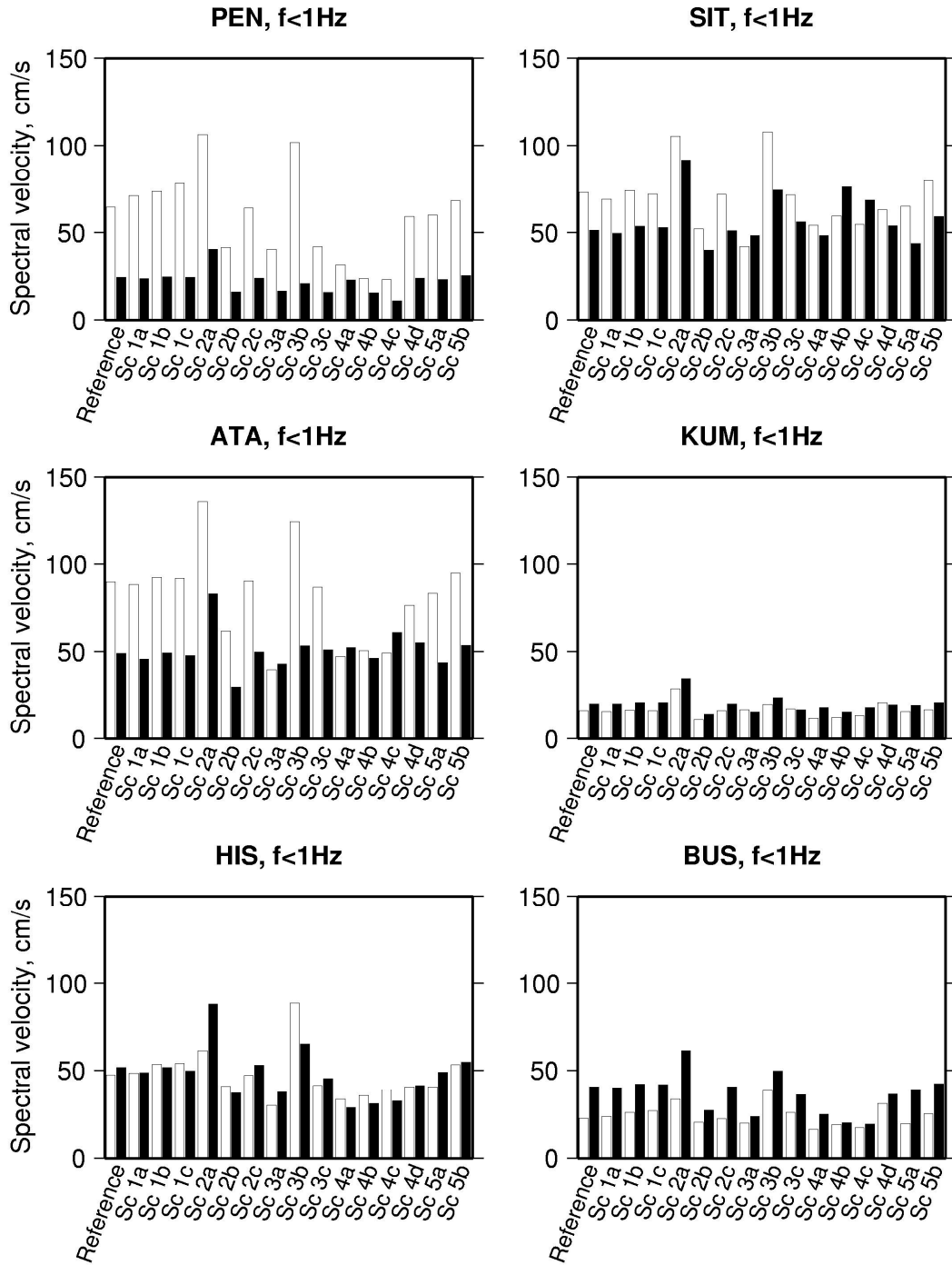
Figure 11.
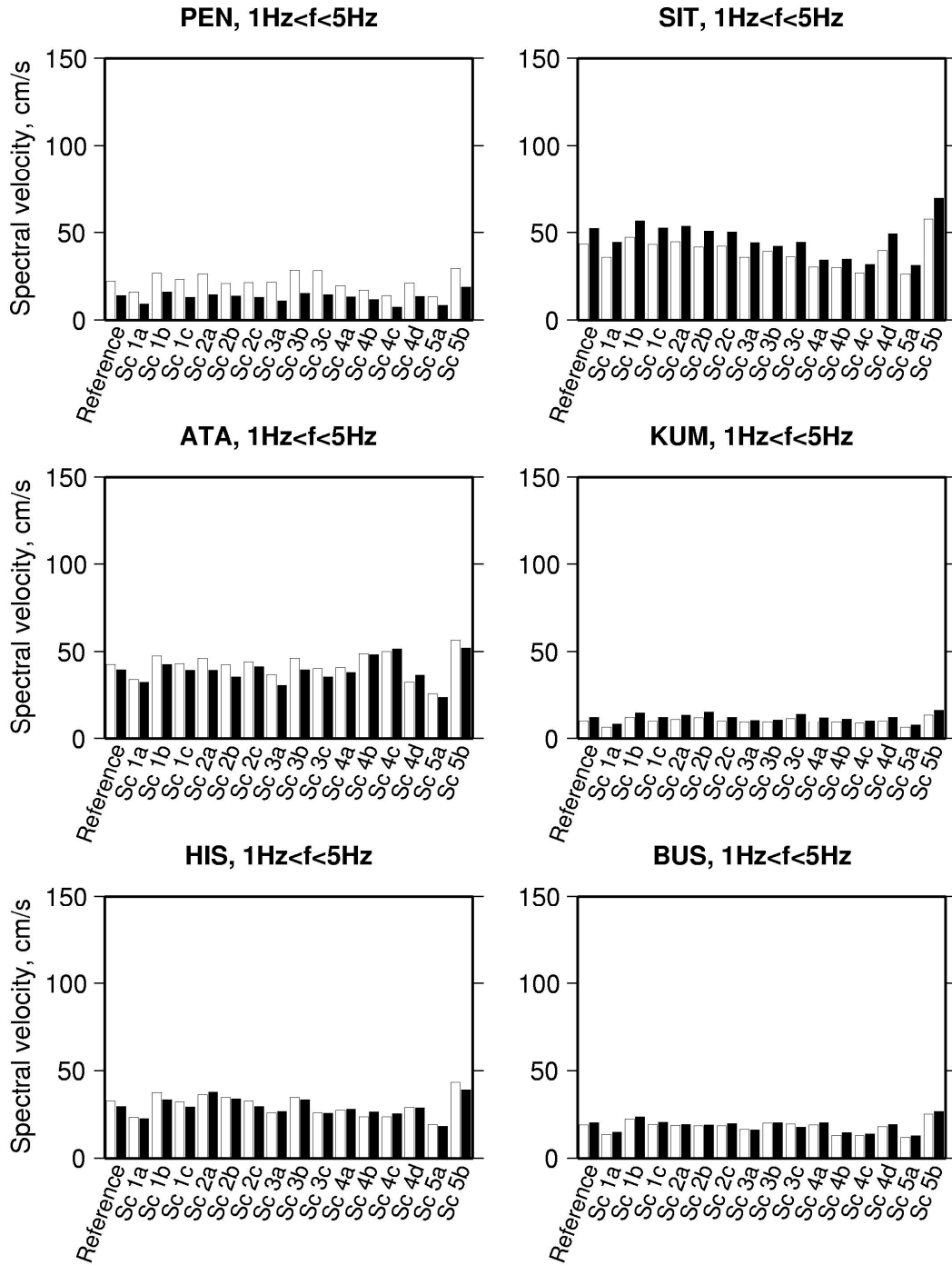
Figure 12.
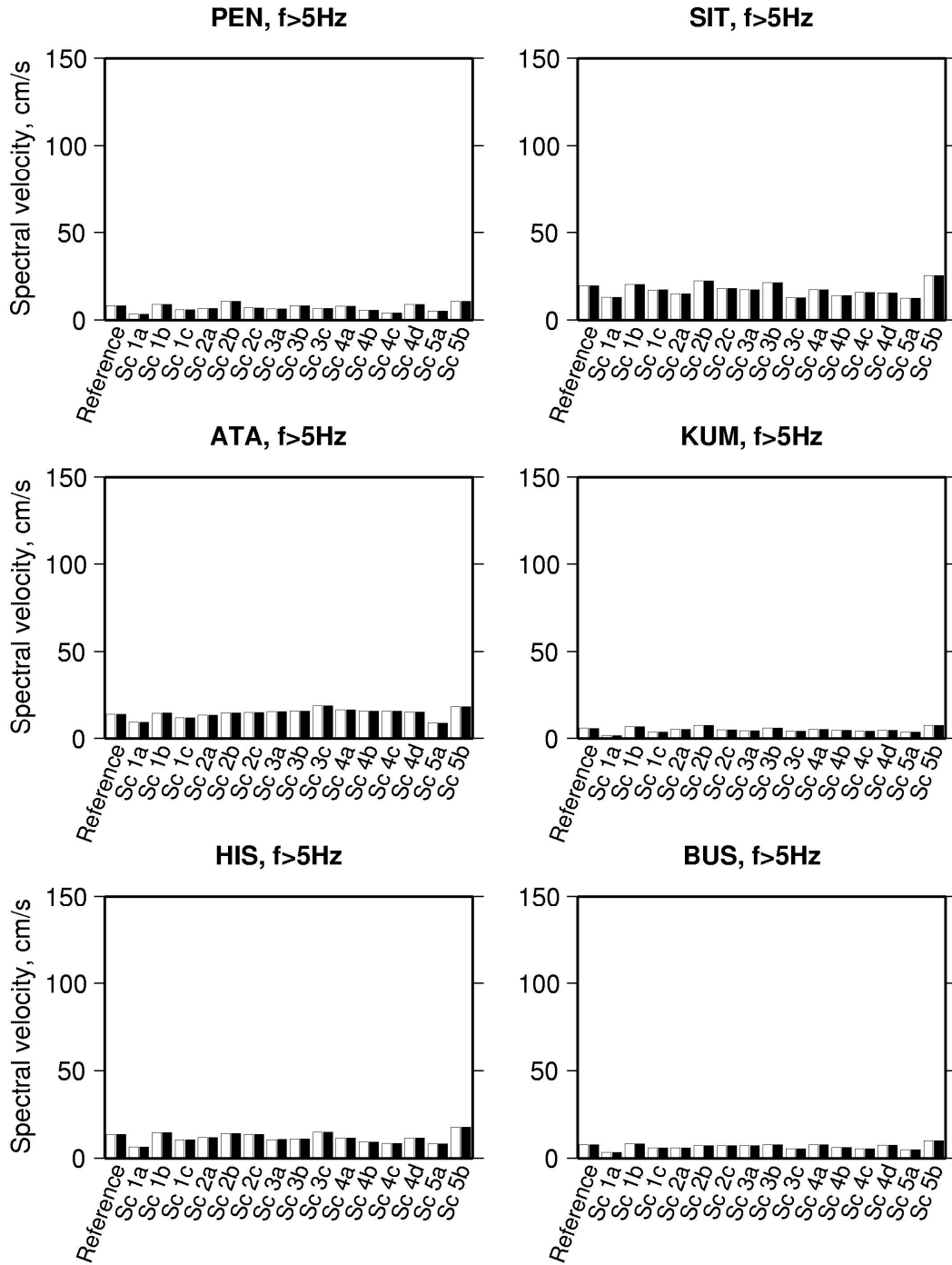
Figure 13.
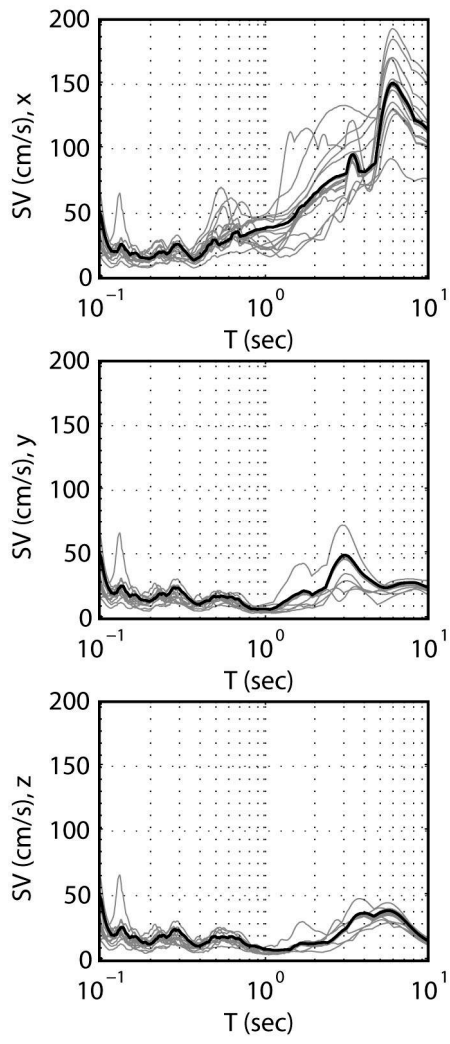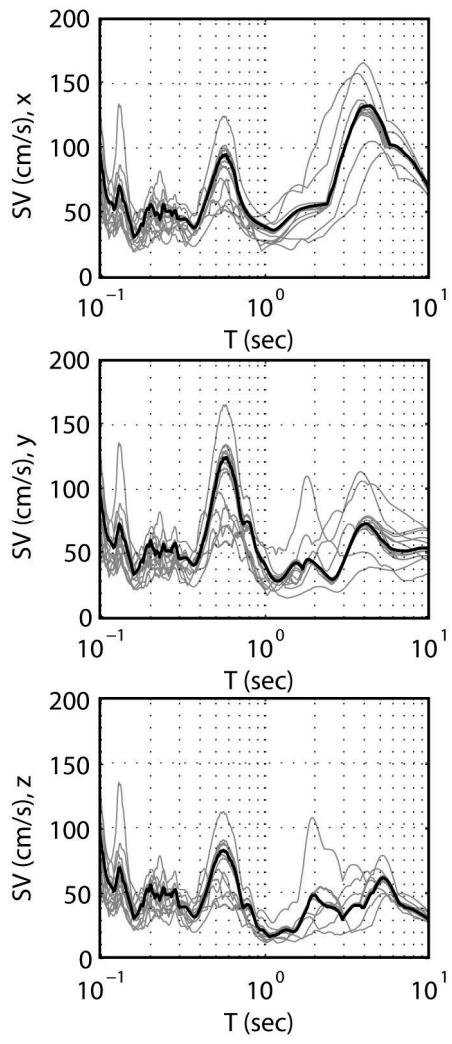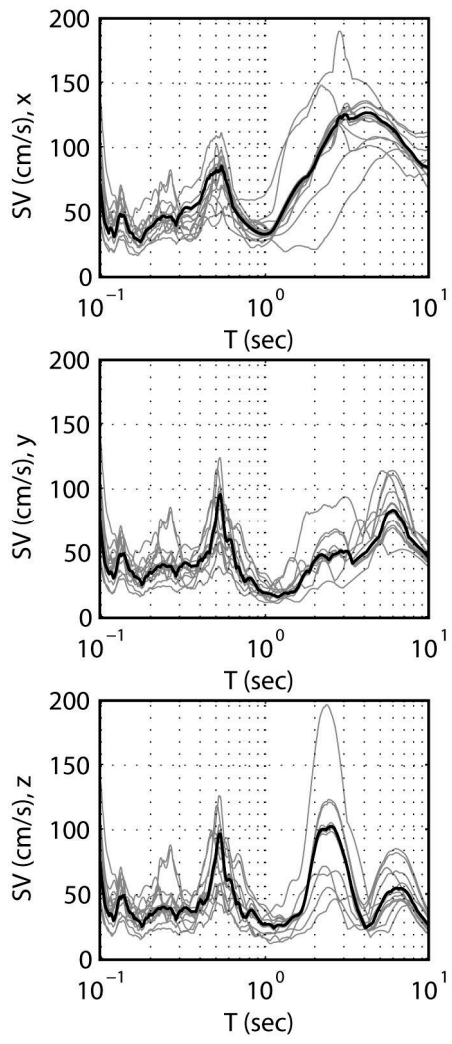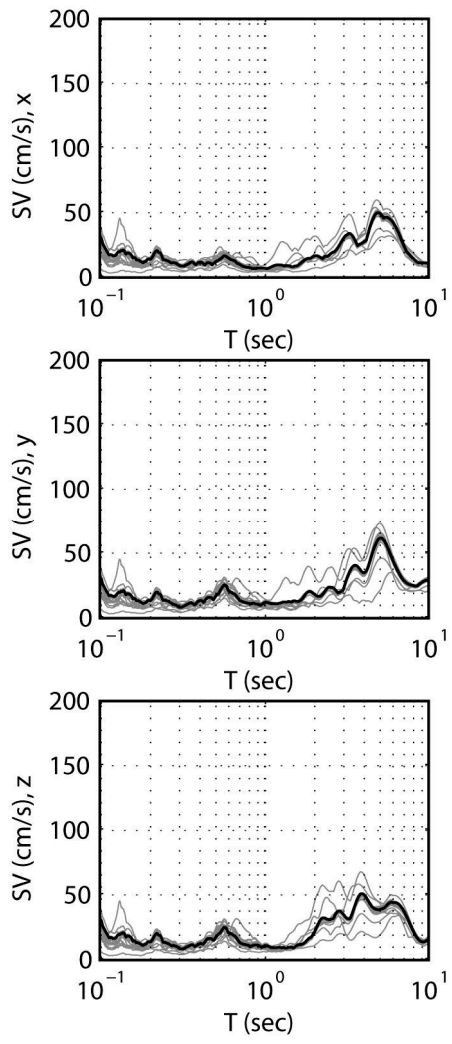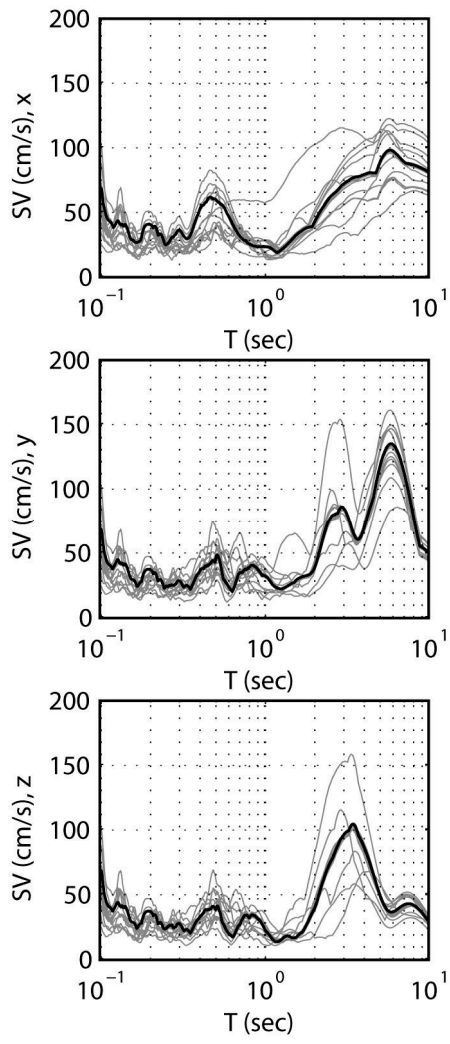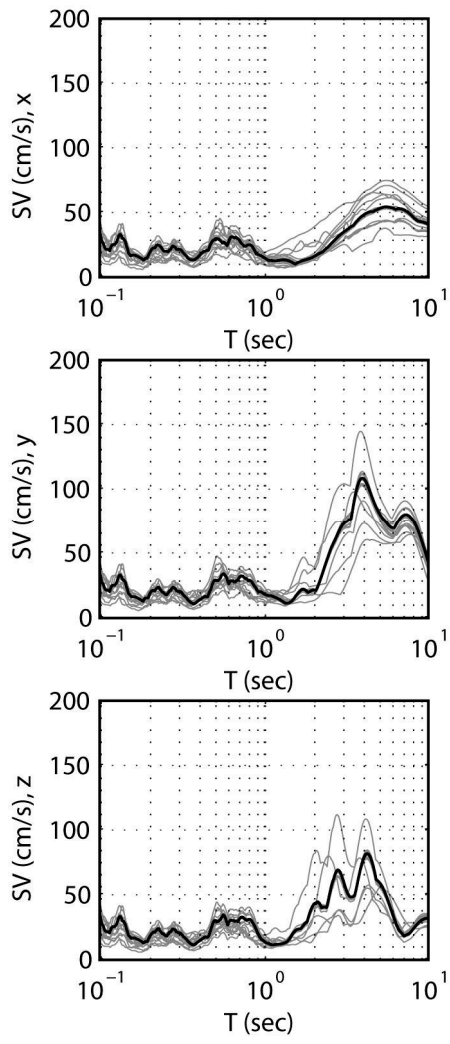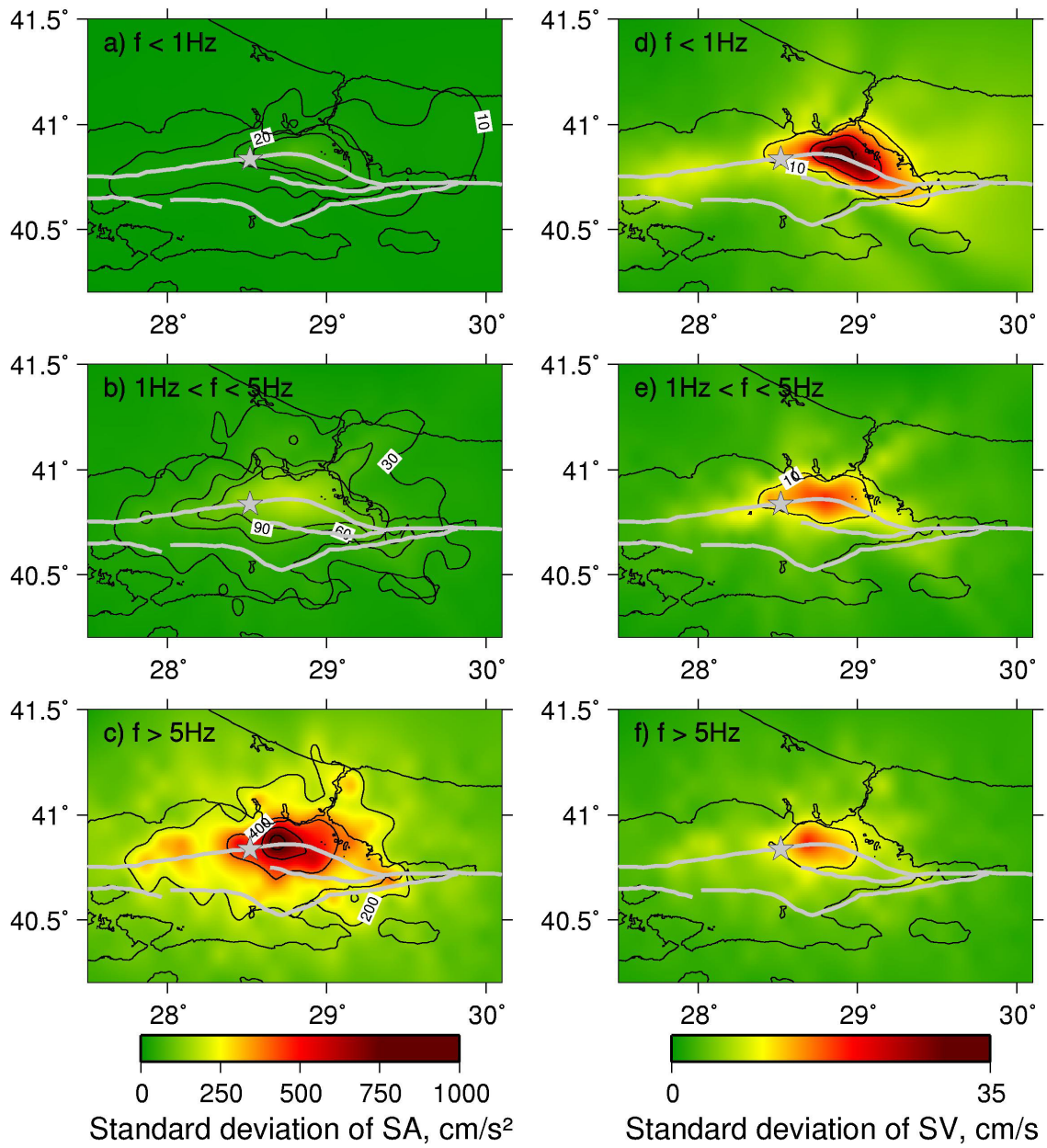
Figure 14a.

Figure 14b.

Figure 14c.

Figure 14d.

Figure 14e.

Figure 14f.

Figure 15.